Supplementary information

Tailoring the Co^{4+}/Co^{3+} active sites in single perovskite as a bifunctional catalyst for oxygen electrode reactions

Song-Jeng Huang [a, +], Adil Muneeb [a, b, + *], Palani Sabhapathy [c], Anji Sheelam [b], Khasim Saheb Bayikadi [b], Raman Sankar [b*]

[a] Department of Mechanical Engineering, National Taiwan University of Science and Technology, No. 43, Section 4, Keelung Road, Taipei 10607, Taiwan, R.O.C.

[b] Institute of Physics, Academia Sinica, Taipei 11529, Taiwan; Center for Condensed Matter Sciences, National Taiwan University, Taipei 10617, Taiwan;

[c] Center for Condensed Matter Sciences, National Taiwan University, Taipei-10617, Taiwan

[+] equal contribution & * corresponding authors

$PrCoO_3$			$Pr_xCa_{1-x}Co_{0.8}Fe_{0.2}O_3$		
Sample			x=0.1	X=0.2	X=0.3
Atomic Coordinates Pr,Ca	x	0.99640	-0.03240	-0.0324	-0.03240
	y	0.02940	0.25000	0.25000	0.25000
	z	0.25000	-0.00710	0.00710	0.00710
Atomic Coordinates O1	x	0.06770	0.50650	0.50650	0.50650
	y	0.49410	0.25000	0.25000	0.25000
	z	0.25000	0.06420	0.06420	0.06420
Atomic Coordinates O2	x	0.71740	0.22030	0.22030	0.22030
	y	0.28310	0.03240	0.03240	0.03240
	z	0.06373	0.78540	0.78540	0.78540
Bond Distances (A)	Co-O1	1.9301	1.93242	1.9324	1.93352
		1.9724	1.95604	1.95559	1.95705
	Co-O2	1.9717	1.91173	1.91147	1.91298
Bond Angles (deg)	Co-O1-Co	158.170	159.267	159.275	159.272
	Co-O2-Co	148.001	159.1845	159.1825	159.1846
Bragg R-factor		9.16 %	6.29 %	5.33 %	13.51 %
RF-factor		16.5%	6.95 %	6.765 %	15.09 %
Chi^2		1.17	1.27	1.10	1.18

Table S1. Structural parameters of the catalysts obtained from Ritveld refinement of XRD powder data

Table S2. Binding energy values of Co^{4+} and Co^{3+} oxidation states in $PrCoO_{3-\delta}$, $Pr_xCa_{1-x}Co_{0.8}Fe_{0.2}O_{3-\delta}$

	Co^{4+}	**Co^{3+}**	**ΔE**
Pure	781.31 ± .06	779.11 ± .02	2.2 ± .08
x=0.1	781.36 ± .01	779.13 ± .02	2.2 ± .03
x=0.2	781.35 ± .04	779.12 ± .01	2.2 ± .05
x=0.3	781.36 ± .05	779.13 ± .02	2.2 ± .07

Table S2. Binding energy values of Co^{4+} and Co^{3+} oxidation states in $PrCoO_{3-\delta,}$ $Pr_xCa_{1-x}Co_{0.8}Fe_{0.2}O_{3-\delta}$

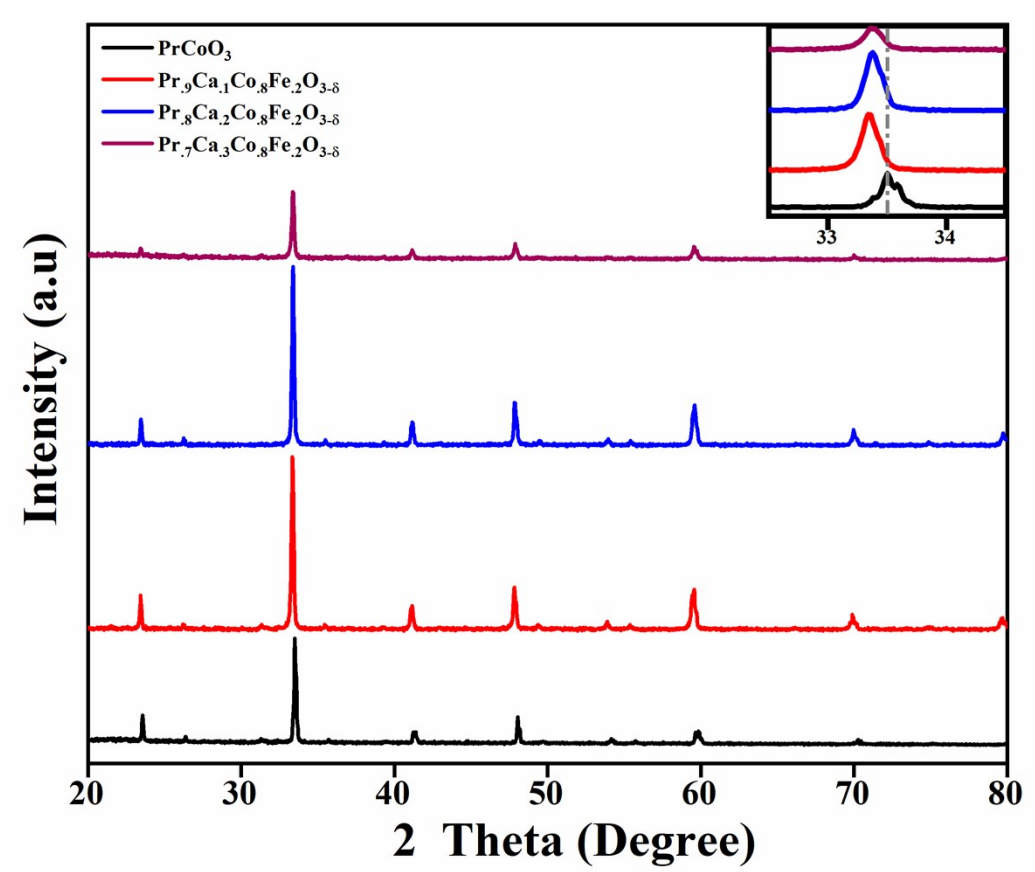

Fig. S1 Powder X-ray Diffraction data of the perovskite catalysts.

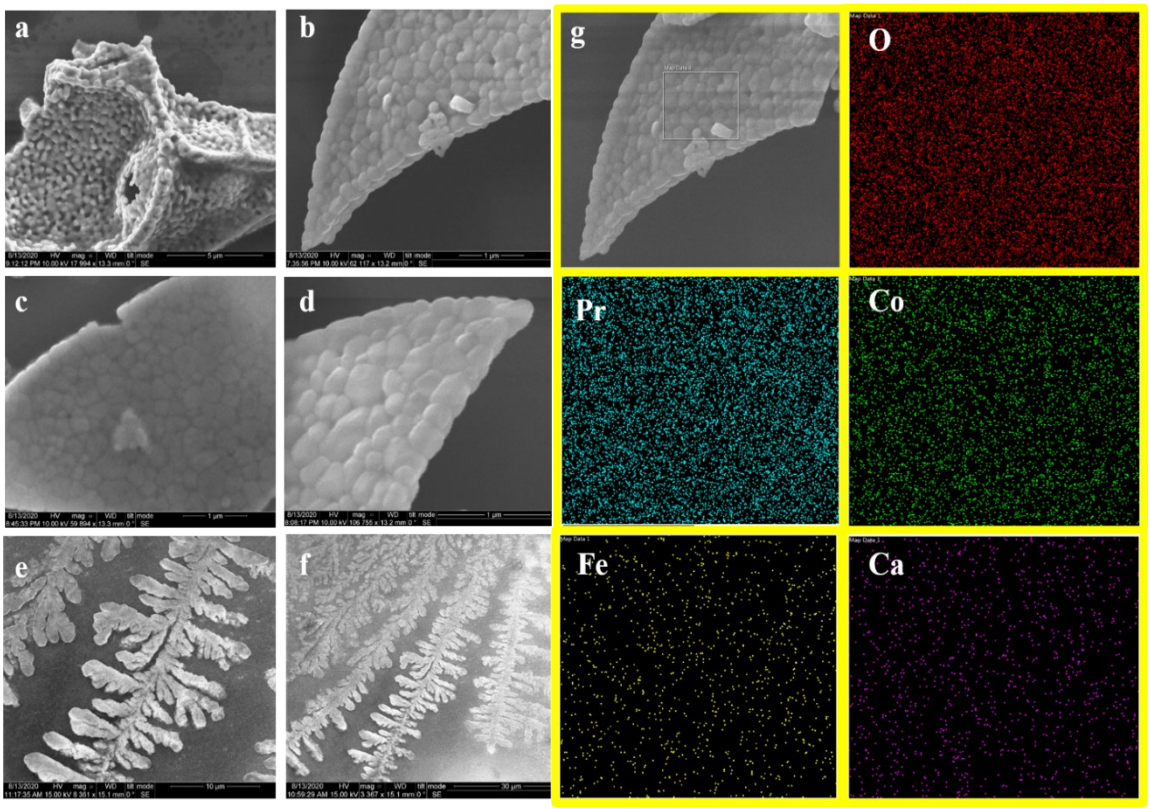

Fig. S2 Scanning electron microscopy (SEM) images of the perovskite catalysts, (a) $PrCoO_{3-\delta}$. (b-d) $Pr_{1-x}Ca_xCo_{0.8}Fe_{0.2}O_{3-\delta}$ (x=0.1-0.2, (e-f) leaf-like micro/nanostructure after self-assembly, and (g) elemental mapping of $Pr_{0.9}Ca_{0.1}Co_{0.8}FeO_{3-\delta}$.

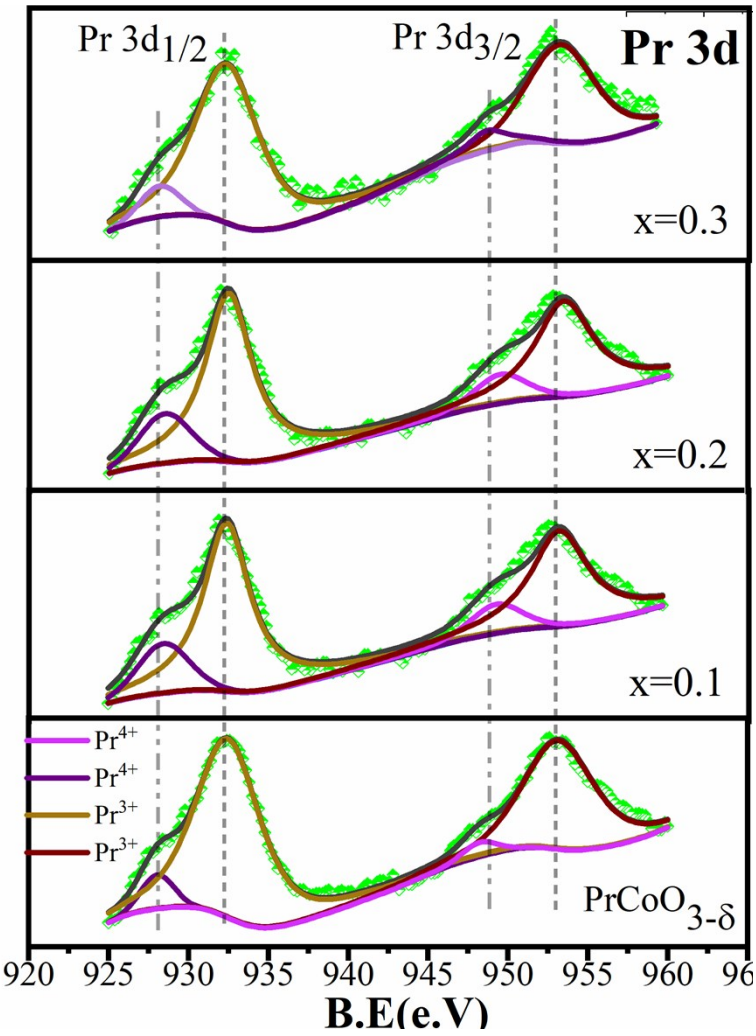

Fig. S3 XPS for Pr 3d spectra of $PrCoO_{3-\delta}$, $Pr_{1-x}Ca_xCo_{0.8}Fe_{0.2}O_{3-\delta}$ (x=0.1-0.3)

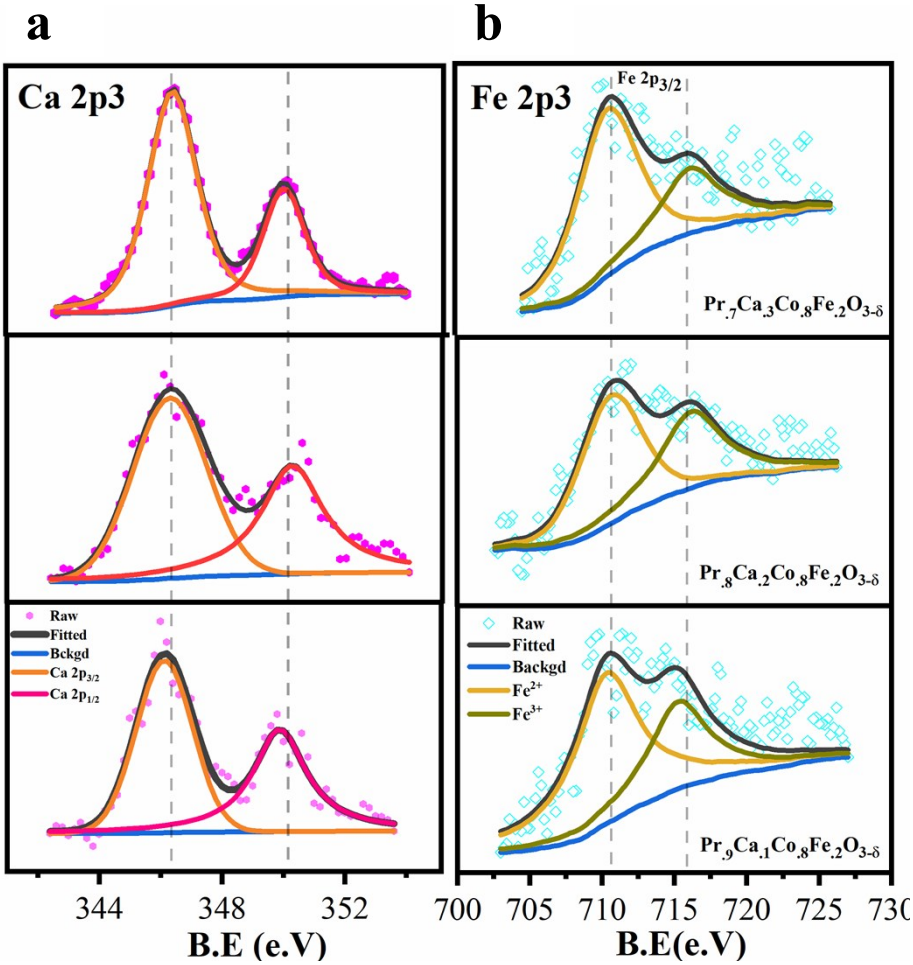

Fig. S4 X-ray photoelectron spectroscopy (XPS) of the perovskite catalysts, (a) XPS for Ca 2p spectra of $Pr_{1-x}Ca_xCo_{0.8}Fe_{0.2}O_{3-\delta}$ (x=0.1-0.3) and (b) XPS Fe 2p spectra of $Pr_{1-x}Ca_xCo_{0.8}Fe_{0.2}O_{3-\delta}$ (x=0.1-0.3).

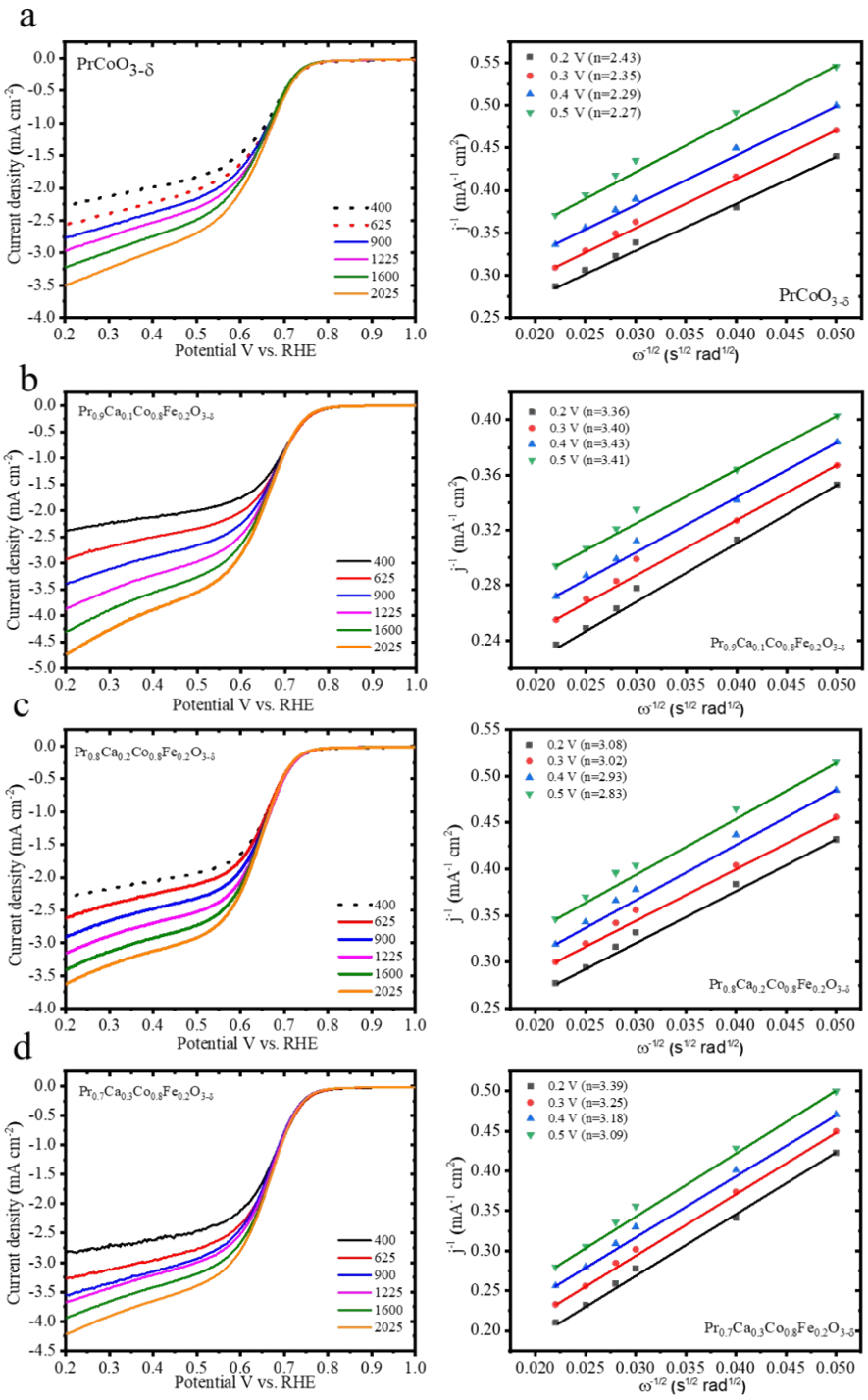

Fig. S5 LSV curves at different rotation speeds along with Corresponding K-L plots at different potentials (a) $PrCoO_{3-\delta}$. (b-d) $Pr_{1-x}Ca_xCo_{0.8}Fe_{0.2}O_{3-\delta}$ (x=0.1-0.3).

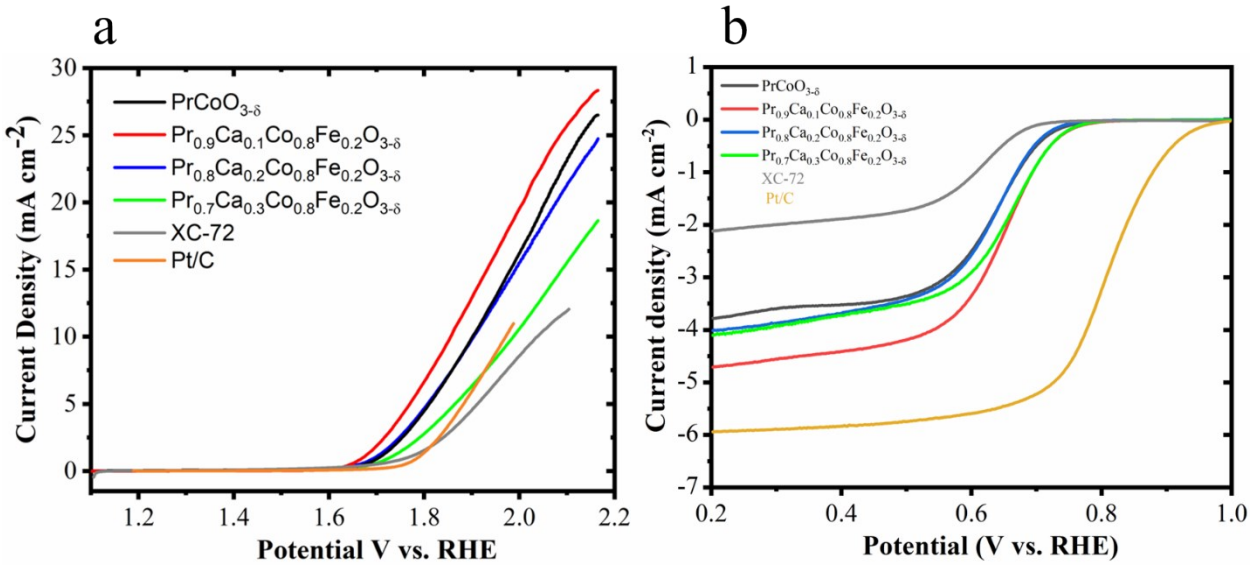

Fig. S6 LSV curves of standard Pt/C and Xc-72 at 1600 rpm (a) OER (b) ORR.